Atmospheric Environment 278 (2022) 119091

Contents lists available at ScienceDirect

Atmospheric Environment

journal homepage: www.elsevier.com/locate/atmosenv

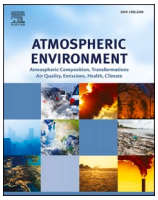

Characterization of chemical and physical changes in atmospheric aerosols during fog processing at Baengnyeong Island, South Korea

Taehyun Park [a], Dong Hee Jung [b], Yongjae Lim [b], Jihee Ban [a], Kyunghoon Kim [a], Seokwon Kang [a], Gyutae Park [a,c], Siyoung Choi [a], Hyunjae Kim [b], Minyoung Sung [b], Yongjoo Choi [a], Alexandra J. Boris [d,e], Jeffrey L. Collett Jr. [d], Taehyoung Lee [a,*]

[a] Department of Environmental Science, Hankuk University of Foreign Studies, Yongin 17035, South Korea
[b] Climate and Air Quality Research Department, National Institute of Environmental Research, Incheon 22689, South Korea
[c] Now at Air Pollution Engineering Division, Climate and Air Quality Research Department, National Institute of Environmental Research, Incheon 22689, South Korea
[d] Department of Atmospheric Science, Colorado State University, Fort Collins, CO, 80521, USA
[e] Now at California Air Resources Board, Sacramento, CA 95811, USA

HIGHLIGHTS

- Particle composition and size measurements were used to explore fog processing.
- Organic scavenging efficiency η (7–34%) was lower in less-oxidized particles.
- Mass decreased after 3 fog events and increased, notably in organics, in 2 events.
- The aerosol carbon oxidation state decreased by the end all fog episodes.

ARTICLE INFO

Keywords:
Fog processing
Scavenging efficiency
Hydroxymethanesulfonate (HMS)
Aqueous secondary organic aerosol (aqSOA)

ABSTRACT

In situ interactions between aerosols and atmospheric fog droplets were explored using aerosol physical and chemical measurements and fog samples taken at the Baengnyeong Island Intensive Air Quality Monitoring Station, South Korea during June 16th to July 21st, 2014. To investigate wet scavenging by fog, aerosols were characterized by aerosol mass spectrometer before, during, and after five fog events. Total non-refractory PM_1 mass decreased by an average of 22.8% with the onset of fog. The scavenging efficiency (η) of organics was 7–34%, where lower η was associated with lower organic oxidation and hygroscopicity. The η was 16–68% for NH_4^+, -1–35% for SO_4, and 17–86% for NO_3^-, consistent with previous studies and the relatively high NO_3^- hygroscopicity. The variation in scavenging was size dependent for both organics and NO_3^-. Particles with lower NO_3^- η on 7/18 were smaller (mode = 346 nm), while those with higher NO_3^- η were larger (593 nm). Differences in mass were also explored before and after fog events. Three episodes showed overall decreases in all the components after the fog event, while two episodes showed overall increases, most notably in organics. Both organic mass and $SO_2^+/H_2SO_4^+$ ratio were used to indicate the prevalence of hydroxymethanesulfonate (HMS), an aqueous secondary organic aerosol (aqSOA) formation marker, which increased after the 7/18 fog episode. The aerosol carbon oxidation state decreased toward the end of all fog episodes suggesting possible molecular fragmentation and loss of highly oxidized functional groups. On 7/18, the organic content developed lower O:C and higher H:C moving "up" a slope of −1 in a van Krevelen diagram over the course of the fog episode, indicating carboxylic acid or hydroxycarbonyl loss. This study explores relatively rare time-resolved aerosol fog processing measurements. The results confirm previously established relationships between scavenging and particle size, demonstrate overall increases and decreases in particle mass after fog processing based on dominant local chemistry and wet deposition, and show predominant decreases in organic oxidation after fog processing, thereby, contributing to our understanding of particle processing and organic cycling in the atmosphere.

* Corresponding author.
E-mail address: thlee@hufs.ac.kr (T. Lee).

https://doi.org/10.1016/j.atmosenv.2022.119091
Received 25 August 2021; Received in revised form 1 March 2022; Accepted 27 March 2022
Available online 28 March 2022

1. Introduction

Fog and cloud processing can influence the fate of atmospheric particulate species, which play important roles in climate and radiative balance (Ghan et al., 2007), air quality, human health (Pope et al., 2002), nutrient cycling (Benedict et al., 2013), and other important biogeochemical processes. Fog processing involves both physical and chemical mechanisms including scavenging and removal of atmospheric particles by droplets, which can serve to reduce particle and gas concentrations in the atmosphere (Collett et al., 2001), hygroscopic particle growth (Tang and Munkelwitz, 1993), aqueous processing such as aqueous oxidation of both gas phase precursors and dissolved semi- and low-volatile compounds (Ervens et al., 2011; Harris et al., 2014; Kaul et al., 2011; Shen et al., 2012), and droplet re-evaporation, which releases both particulate and gaseous species (Ervens, 2015). Fog and cloud droplets also play a vital role in the hydrological cycle and influence atmospheric radiative transfer (Pruppacher and Klett, 2010). Fogs comprise of a complex multiphase system combining gases, particles, and water droplets.

Fog scavenging of particles includes impaction and nucleation mechanisms. Impaction scavenging involves the inclusion of interstitial particles into fog droplets via Brownian diffusion, inertial impaction, and phoretic processes, while nucleation scavenging involves the absorption of water by particles to become activated fog droplets in a supersaturated environment (van Pinxteren et al., 2016). Numerous studies have found preferential scavenging of species with higher hygroscopicity including NO_3^- (Gilardoni et al., 2014; Varutbangkul et al., 2006) and more-oxidized organic compounds (Decesari et al., 2005; Noone et al., 1992). Our understanding of changes in particle chemical composition, especially the organic fraction, due to fog processing continues to develop and will benefit from additional ambient observations (Herckes et al., 2013).

Scavenging is also a function of particle size both in total and for individual species featuring various size-scavenging relationships. For example, Gilardoni et al. (2014) found a size-segregated scavenging efficiency (η) following sigmoidal curves for both NO_3^- and organic aerosols with η decreasing to near zero with decreasing vacuum aerodynamic diameter (d_{va}) below 100 nm and increasing to ~1 at d_{va} values of above 700 nm. Other studies have also found size dependencies even though they were not resolved by particle composition (Noone et al., 1992; Sellegri et al., 2003). Overall, few studies have investigated compositionally resolved fog scavenging as a function of particle size.

However, scavenging of particles by fog droplets when fog event first impacts the study site is only one of the many processes that affect particle mass and composition during fog processing. For instance, aqueous reactions can both produce and consume gaseous and particulate species, and subsequent fog droplet evaporation may release some of these species in the form of physicochemically altered particles. Such aqueous secondary aerosol formation can be indicated by increases in particle size within the 0.4–1 μm range (Hering and Friedlander, 1982; John et al., 1990) in contrast to gas-phase particle formation, which predominantly forms particles of <0.2 μm (Ervens et al., 2011). Aqueous secondary organic aerosol (aqSOA) formation can be indicated by the detection of methane sulfonic acid (MSA), which is produced by the oxidation of dimethyl sulfide (DMS) emitted from oceanic organisms (Phinney et al., 2006; von Glasow and Crutzen, 2004; Zorn et al., 2008).

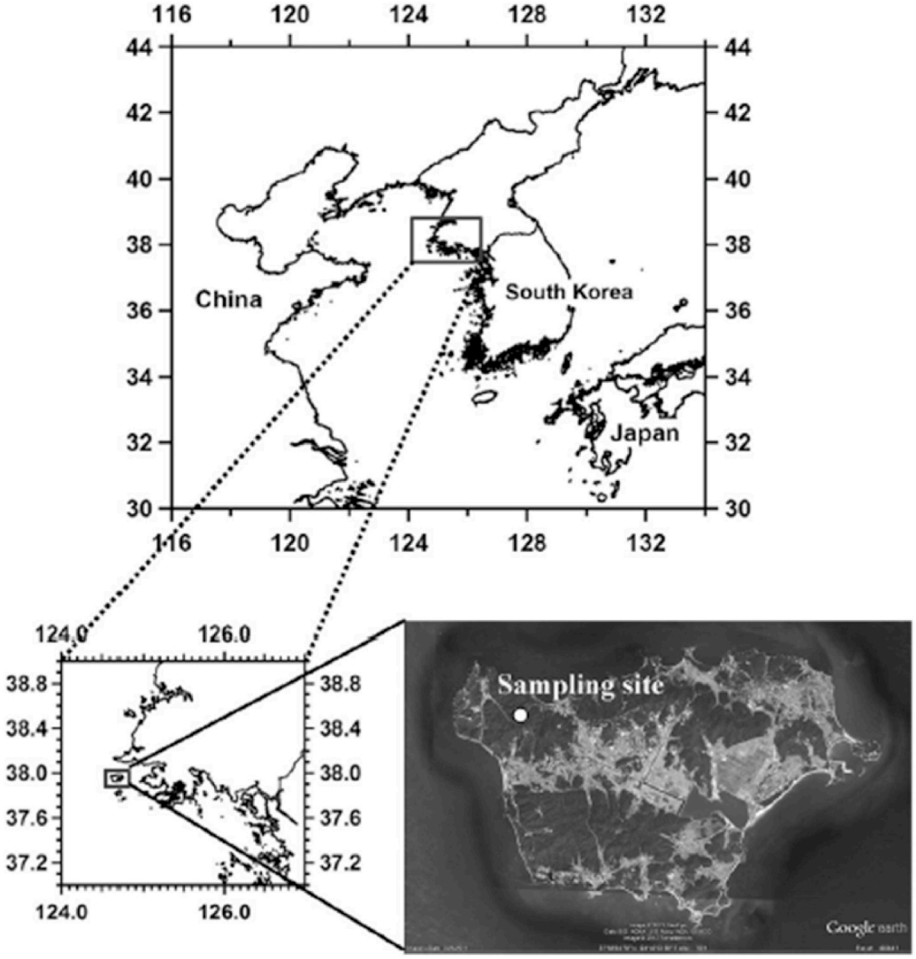

Fig. 1. Location of the Baengnyeong Island sampling site in South Korea. Reproduced with permission from Lee et al. (2015).

Table 1
The summary of five-fog events and the meteorological data. The 1 min meteorological data produced from the Automated Synoptic Observing System (ASOS) operated by Korea Meteorological Administration (KMA) on Baengnyeong Island (37.97 °N, 124.71 °E). All the datasets averaged depending on the period.

Date (2014)	Period	Time (Local)	Temperature[a] (°C)	Wind direction[a] (°)	Wind speed[a] (m s^{-1})	Relative humidity[a] (%)	LWC (mg m^{-3})
June 30th	Before	02:30–03:00	20.6	251.7	1.35	95.4	3.9
	During	03:00–08:00	20.3	211.5	1.82	98.1	34.6
	After	08:00–08:30	21.5	143.7	0.98	97.6	3.5
July 1st	Before	02:30–03:00	21.2	156.3	0.67	97.8	3.4
	During	03:00–11:15	20.6	141.5	3.14	96.1	25.1
	After	11:15–11:45	22.4	133.6	3.81	86	3.4
July 2nd	Before	03:00–03:30	20.8	139.5	4.17	95.3	2.7
	During	03:30–11:45	19.7	96.4	5.87	98.3	84.0
	After	11:45–12:15	20.9	103.7	6.81	98.5	2.8
July 18th	Before	00:30–01:00	22.8	161.2	3.09	96.7	0.7
	During	01:00–10:45	21.6	115.9	4.33	99	56.6
	After	10:45–11:15	23.2	106.4	4.94	99.6	NA[b]
July 20th	Before	00:30–01:00	23.5	205.3	4.09	97.7	0.5
	During	01:00–12:00	23.7	155.9	2.97	95.1	24.4
	After	12:00–12:30	26.9	204.3	5.34	73.4	NA

[a] The ASOS data from KMA (https://data.kma.go.kr/).
[b] NA: not available.

In addition, oxalic acid is a typical marker of aqSOA formation by the oxidation of glyoxal and other gas-phase precursors (Carlton et al., 2007; Crahan et al., 2004). Another aqSOA formation tracer, hydroxymethanesulfonate (HMS) is an important tracer in ambient fog and cloud processing. HMS is produced by the formaldehyde–HSO_3^- (or SO_4^{2-}) reaction in aqueous-phase (Gilardoni et al., 2014; Munger et al., 1986; Whiteaker and Prather, 2003).

To better understand particle chemical composition and the interactions between aerosols and atmospheric droplets, fog sampling and aerosol physical and chemical measurements were conducted at the Baengnyeong Island Intensive Air Quality Monitoring Station, South Korea, during June–July 2014. The chemical composition and physical properties of aerosol particles were characterized before, during, and after fog events using a high-resolution time-of-flight aerosol mass spectrometer (HR-ToF-AMS, Aerodyne) and a scanning mobility particle sizer (SMPS, TSI). The collected fog/cloud samples were also characterized and are presented separately (Boris et al., 2016). This work will examine changes in particle chemical composition and microphysics due to fog and cloud processing in the boundary layer.

2. Methods

2.1. Sampling site

The interstitial particles in the fog and ambient particles were measured at the Baengnyeong Island Intensive Air Quality Monitoring Station, South Korea (37.97 °N, 124.63 °E; 150 m above mean sea level (AMSL); Fig. 1) during June 17th to July 21st, 2014. This site, which houses a variety of instruments and is used by the National Institute of Environmental Research (NIER) for routine air quality monitoring, is located on a relatively small and low-lying island at the northwestern-most boundary of South Korea and features frequent fog events and well-studied atmospheric chemistry. Baengnyeong Island is influenced by both photochemically aged and somewhat less-oxidized transported industrial emissions, biomass burning and dust from the Pearl River Delta (generally more aged and richer in SO_4^{2-}), Korean Peninsula and East sea (typically containing more abundant organics), and East China Sea (Boris et al., 2016; Choi et al., 2016; Kang et al., 2018, 2020; Lee et al., 2015).

2.2. Instrumentation and data analysis

The particle chemical composition was characterized before, during, and after fog events using a HR-ToF-AMS in the V-mode with an averaging time of 5 min. Ambient air was drawn from an inlet ~100 m above sea level at a total flow rate of 3 LPM through a URG cyclone (D_{50} = 2.5 μm) and dried to < 40% RH using Perma Pure dryers (MD-110-24) before being focused into the AMS interior via an aerodynamic lens (aerodynamic diameters = 60–600 nm; Liu et al., 2007). Within the AMS, particles are vaporized at 600 °C, ionized at 70 eV, and the resulting fragmented molecules are separated by mass in a ToF-MS and counted to produce time-resolved mass spectra (DeCarlo et al., 2006). In this study, total organics, SO_4^{2-}, NO_3^-, NH_4^+, and Cl^- were quantified using the standard fragmentation tables and adjustments for composition-dependent collection efficiency (Allan et al., 2004; Middlebrook et al., 2012) provided in SQUIRREL (v1.56C) and PIKA (v1.15C) AMS data analysis software (DeCarlo et al., 2006; Sueper, 2009). Although fragmentation limits our ability to determine organic speciation, some speciation was explored (discussed in Section 3.5) and elemental analysis was used to investigate changes in organic aerosol oxidation state (including O/C, H/C, and OM/OC) during fog processing. Ammonium nitrate particles (300 nm, ~350 particles cm^{-3}) were used for NO_3^- ionization efficiency (IE) calibrations, and default relative IE values were used for other species.

Positive Matrix Factorization (PMF) analysis was performed on the AMS data using the Igor Pro-based PMF Evaluation Toolkit (PET; v3.05). PMF has been described in detail elsewhere (Paatero and Tapper, 1994; Paatero, 1997; Ulbrich et al., 2009). Ulbrich et al. (2009) and others have previously applied PMF to AMS data using PET, which deconvolves spectral patterns, or 'factors' (such as hydrocarbon-like organic aerosol, biomass burning aerosol, and oxidized organic aerosol, or OOA) from the measured mass spectra and constructs a representative spectrum and timeline for each factor (e.g., Jimenez et al., 2009; Ulbrich et al., 2009; Sun et al., 2011; Zhang et al., 2011; Saarikoski et al., 2012; Lee et al., 2015). Descriptive statistics for the PMF analysis (i.e., FPEAK and Q values) were provided in Fig. S1.

Aerosol physical properties were measured using a scanning mobility particle sizer (SMPS, model 3034, TSI Inc., USA) with a particle size scanning range of 10.4–469.8 nm and scanning time of 5 min as described in Hogrefe et al. (2006). The SMPS was preceded by a krypton-85 (^{85}Kr) neutralizer (model 3077, TSI Inc., USA).

The fog liquid water content (LWC) was measured by a Gerber particulate volume monitor (PVM-100, GSI INC., USA; Gerber, 1991) and the fog event was determined as periods in which the LWC exceeded 30 mg m^{-3} (Boris et al., 2016). The World Meteorological Organization (WMO) defines fog by thickness (or intensity) according to the restriction of horizontal visibility. The visibilities of dense, moderate, and light fogs are less than 1 km, 1 to less than 5 km, and 5 to less than 11 km,

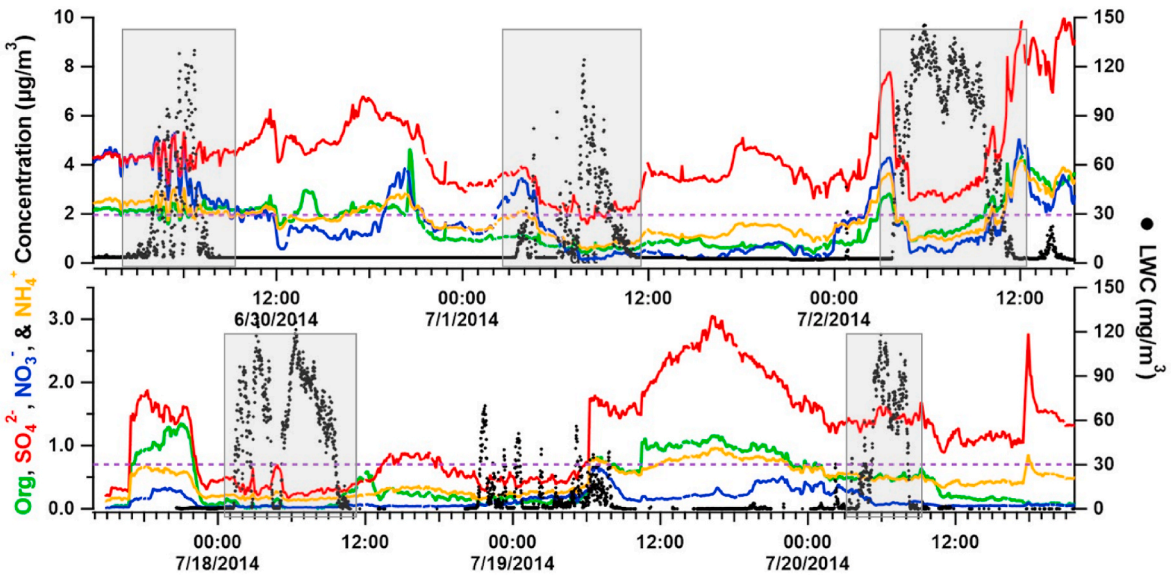

Fig. 2. Timeline of (left axis) particle component concentrations and (right axis, dashed black line) liquid water content; the light purple horizontal line indicates LWC = 30 mg m^{-3}. The period of fog events was provided in Table 1. The gray boxes mean that emphasis of the fog episode in the timeline. (For interpretation of the references to colour in this figure legend, the reader is referred to the Web version of this article.)

respectively (Croft and Ward, 2015). The 30 mg m^{-3} of LWC specified in this paper is the visibility of about 550 m, which corresponds to dense fog (Elias et al., 2015).

The meteorological data were not directly measured. The 1-min meteorological data were produced from the Automated Synoptic Observing System (ASOS) operated by Korea Meteorological Administration (KMA) on Baengnyeong Island (37.97 °N, 124.71 °E) (Table 1) (Korea Meteorological Administration, 2022). Among the ASOS meteorological data, temperature, humidity, wind direction, and wind speed were used for data analysis.

3. Results and discussion

3.1. Liquid water content and chemical composition of fog samples

Fog events (LWC >30 mg m^{-3}) impacted the monitoring station on 6/30, 7/1, 7/2, 7/3, 7/18, 7/19, and 7/20 of 2014. Of these seven events, the data processing herein focuses on five, namely episodes on 6/30, 7/1, 7/2, 7/18, and 7/20 (Table 1). The 7/3 and 7/19 episode was excluded from the analysis because the LWC exceeded 30 mg m^{-3} only intermittently. The compositions of these fog water samples are reported in depth in Boris et al. (2016) and they are summarized here. Boris et al. (2016) collected and analyzed fog samples, which were larger than 16 μm, and small droplets in the range of 4–16 μm. Overall, the dominant components of the fog water were NH_4^+ (mean = 2220 μM), NO_3^- (1260 μM), SO_4^{2-} (730 μM), Na^+ (551 μM), Cl^- (253 μM), and the fog water pH was 3.48–5.00 (3.94). Marine sources as indicated by Ca^{2+} and other species from sea-salt and biomass burning as suggested by K^+ in conjunction with nitrophenol, possible levoglucosan enhancement (Weber et al., 2007), and fire detected upwind (via MODIS and meteorological analysis) contributed considerably to particulate mass on some dates (Boris et al., 2016).

Acetic, formic, oxalic, succinic, maleic, and other organic acids are often formed from aqueous reactions and contribute significantly to the fog water organic fraction, indicating the influence of aqueous (in addition to dry) photochemical oxidation during long-range transport (Boris et al., 2016).

3.2. Time series of non-refractory PM_1 mass and chemical composition

Fig. 2 shows the variations in non-refractory PM_1 (NR-PM_1) component mass during the five fog episodes explored in this study. The total average NR-PM_1 (NR-PM_1 = Organics, SO_4^{2-}, NO_3^- and NH_4^+) concentration with standard deviation was 6.30 ± 4.26 μg m^{-3} during on June 17th to July 21st, 2014. SO_4^{2-} and organics were the predominant aerosol species at 1–11 μg m^{-3} (48.6 ± 12.1%) and 1–7 μg m^{-3} (23.0 ± 12.7%), respectively. NO_3^- and NH_4^+ were lower at 0.2–4 μg m^{-3} (10.5 ± 7.42%) and 0.3–4 μg m^{-3} (17.8 ± 3.57%), respectively. NH_4^+ was higher than NO_3^-, which implies that the NH_4^+ can also combine with SO_4^{2-}. These total particle mass and percent composition values are consistent with previous measurements at this site (Lee et al., 2015) and are similar to those of other marine and anthropogenically influenced coastal sites (Choi et al., 2017; Rivellini et al., 2017; Schulze et al., 2018).

Positive matrix factorization (PMF) analysis of earlier data from Baengnyeong Island indicated the presence of hydrocarbon-like organic aerosol (HOA) and two oxidized organic aerosol (OOA) factors, namely, more oxidized (MO-OOA) and less oxidized (LO-OOA) OOA (Lee et al., 2015). The HOA contributed just 21% of the organic mass on average, and MO-OOA was about three times more abundant than LO-OOA (Lee et al., 2015). In this study, O:C averaged 0.71 ± 0.14 (range: 0.08–0.96) and H:C averaged 1.27 ± 0.10 (range: 0.86–2.10) indicating that the organic aerosol was predominantly within the low-volatility oxygenated organic aerosol (LV-OOA) range as defined in previous studies (Aiken et al., 2008; Canagaratna et al., 2015; Kroll et al., 2009; Ng et al., 2010). The relationships between organic oxidation (and thus, hygroscopicity) and scavenging are discussed in Section 3.3.

3.3. Fog aerosol scavenging efficiency and aerosol changes after fog processing

Total NR-PM_1 averaged 4.86 ± 4.36 μg m^{-3} during fog episodes and 6.30 ± 4.26 μg m^{-3} during non-fog periods. Particle concentrations generally decreased (average decrease = 22.8%) with the onset of the fog episodes (see Fig. 2), which is consistent with previously measured scavenging behavior by Collett et al. (2001) and Gilardoni et al. (2014), who measured 60% reduction in NR-PM_1 during fog events at a background site.

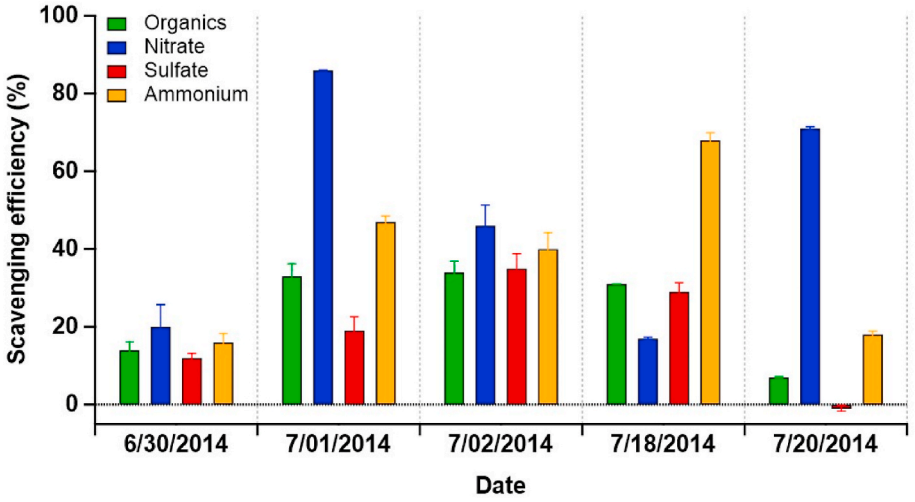

Fig. 3. Scavenging efficiencies of organics, NO_3^-, SO_4^{2-}, and NH_4^+ during each of the fog episodes.

The fog scavenging efficiency (η) is defined as the fraction or percentage of a given particle component X remaining in the atmosphere immediately after the onset of the fog event (Eqn 1) (Noone et al., 1992).

$$\eta = 1 - \frac{[X]_{interstitial}}{[X]_{before\ fog}} \quad \text{(Eq. 1)}$$

where $[X]_{interstitial}$ refers to the concentration of unscavenged particles suspended between fog droplets. We used 30-min average data for the fog scavenging efficiency calculations. [X]*before fog* data was used "before period" datasets in Table 1, and [X]*interstitial* data was used 30-min averaged data right after of "before fog period" in Table 1. Fig. 3 shows the η of each particle constituent during each of the fog episodes. NO_3^- is scavenged most efficiently. Note that the very slight increase in SO_4^{2-} on 7/20 is well within the instrument error. However, this lack of decrease in particulate SO_4^{2-} concentration is atypical of the fog process, and it may indicate the arrival of a new and higher SO_4^{2-} air mass with the fog event. In addition, by checking the wind direction of the 7/20 case, the air masses came from the sea southwest of the monitoring site before the fog event, but during the fog event, the air masses came from inland of the island by the southeast wind (Table 1). The significant differences in η between the components during some of the fog events suggest external mixing and differences in hygroscopicity and or size-dependent composition within the particle population, assuming that the fog events were not accompanied by transported air masses that differed significantly in composition from the pre-fog air masses. For instance, on 6/30 and 7/2, the η patterns of NH_4^+ and NO_3^- are similar, but somewhat (not statistically) different from the scavenging efficiencies shared by organics and SO_4^{2-}. This may indicate externally mixed NH_4NO_3 and Org (organics)-SO_4 (or Org–SO_4–NH_4) particles, of which NH_4NO_3 is scavenged more efficiently.

The Org η values measured herein range from 7% to 34% and include two values of <20%, which are slightly lower than the Org η values measured elsewhere. For instance, η was measured at 20–60% in the Po Valley, Italy (Gilardoni et al., 2014), 33–90% in Angiola, California, and 41% in Fresno, California (Collett et al., 2008). These instances of relatively low organic aerosol scavenging efficiency may have arisen from lower organic hygroscopicity, which can be a characteristic of less-oxidized organic particles (Ge et al., 2012; Lambe et al., 2011; Massoli et al., 2010). Indeed, during the 7/20 episode, which featured particularly low organic scavenging, the particles had relatively high H:C (1.42) and low O:C (0.47) values as compared to the other fog events. The η for ammonium measured 16–68%, while that for SO_4^{2-} ranged from −1 (indicating a slight increase in mass) to 35%. The NO_3^- η values measured herein were 17–86% (average = 48%). The higher values are consistent with NO_3^- scavenging observed in the Po Valley, Italy, where

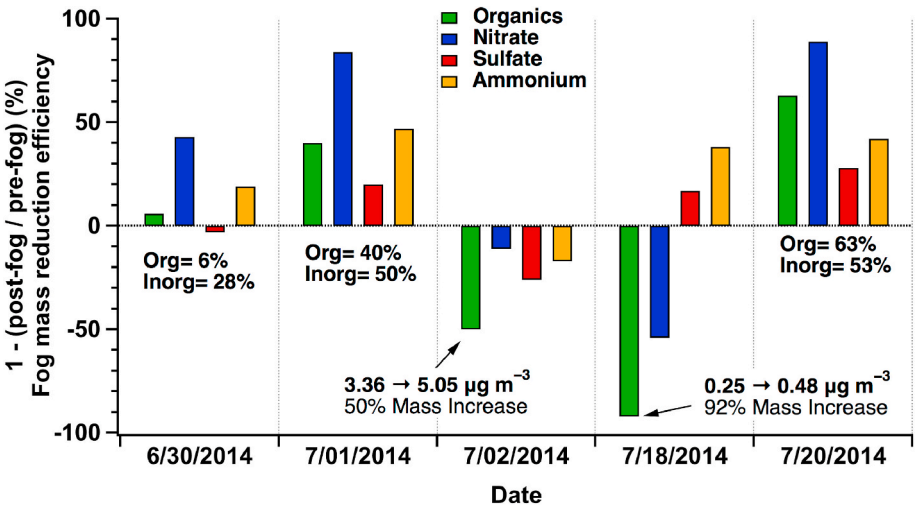

Fig. 4. Overall mass reduction efficiency in Org, NO_3^-, SO_4^{2-}, and NH_4^+ from before to after each fog episode. This metric is similar to scavenging efficiency, but covering the entire fog episode instead of just the initial fog onset. Negative numbers indicate overall mass formation for the given species.

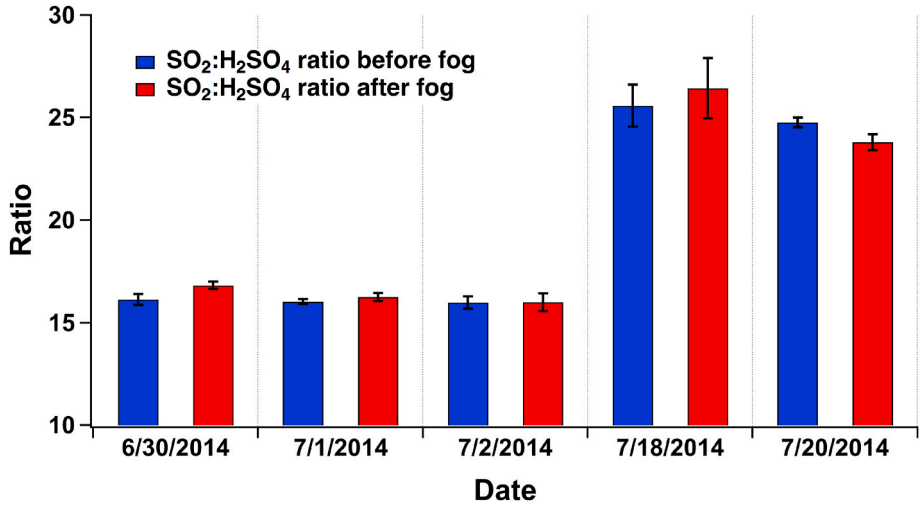

Fig. 5. $SO_2^+/H_2SO_4^+$ ratios before and after the fog episodes.

it averaged 71% (Gilardoni et al., 2014). For both Org and NO_3^-, the variation in scavenging may be size dependent. Gilardoni et al. (2014) found significant decreases in Org and NO_3^- scavenging efficiencies with decreasing size of particles <400 nm and <300 nm, respectively. Indeed, the particle sizes had a mode of 346 nm on 7/18 (Fig. S4) when the lowest NO_3^- η values was observed, and a larger mode of 593 nm during the 7/1 event when NO_3^--η was the highest.

However, scavenging, which reveals the net uptake of particles when the fog event first impacts the study site, is not the only process that affects the ultimate particle mass and composition during fog processing. Aqueous reactions can both produce and consume gaseous and particulate species, and subsequent fog droplet evaporation will release some of these species in physicochemically altered aerosol particles. To explore such processing, and assuming negligible change in aerosol properties due to air mass transport during the given events, Fig. 4 shows the overall mass reduction efficiency (in which, like η, negative numbers denote increases in mass) for Org, NO_3^-, SO_4^{2-}, and NH_4^+ during each of the fog episodes. Note that, while three episodes feature overall decreases in the masses of the chemical components after the conclusion of the fog event, two episodes (namely 7/2 and 7/18) show overall increases in the component masses after the event, despite the initial scavenging (Fig. 4). Organics increase most notably, which is consistent with the increases in SOA due to fog processing found in India (Kaul et al., 2011) and California (Ge et al., 2012). The mass of NO_3^- also increases with organics after fog processing on both 7/2 and 7/18. Farmer et al. (2010) reported that the NO^+/NO_2^+ ratio was increased with the organonitrate. The NO^+/NO_2^+ ratio was increased after fog event on 7/2 case (Table S1), but not 7/18. The increase of organics and NO_3^- on 7/2 case it possibly affected by organonitrate formation. The reduction efficiency of 7/18 case may have been overestimated due to the low concentration (Fig. 4). This finding is consistent with numerous observations showing that aqueous reactions in atmospheric droplets can form secondary organonitrate-containing particles (Ervens et al., 2011; Zhao et al., 2013).

3.4. Hydroxymethanesulfonate indicates aqueous-phase secondary organic aerosol formation

The aqueous-phase reaction can produce many kinds of compounds, such as MSA, oxalic acid, and HMS by a variety of chemical reactions (Carlton et al., 2007; Crahan et al., 2004; Munger et al., 1986; Phinney et al., 2006; Zorn et al., 2008). HMS, a tracer for one route of aqSOA formation, was analyzed to further explore the possible aqSOA formation found in the previous section. HMS formation rate is 1.6 nM h^{-1} to 0.1 M h^{-1} at pH 3 to pH 7, respectively (Munger et al., 1986), and the fog

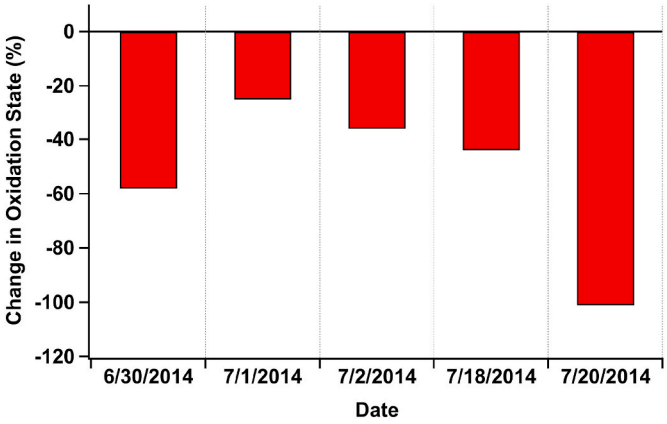

Fig. 6. Change in carbon oxidation state between just before and after the fog event.

water pH was 3.48–5.00 (3.94) during the fog event (Boris et al., 2016). HMS fragments form AMS mass spectra dominated by fragments such as CHO^+, CH_2O^+, SO^+, and SO_2^+, which are common to a variety of ambient aerosol types. No characteristic HMS ions were found in AMS spectra (Ge et al., 2012). However, HMS does not produce SO_3^+, HSO_3^+, or $H_2SO_4^+$ ions under AMS ionization, while ammonium sulfate does. Thus, we can use the changes in SO^+/SO_3^+, SO^+/HSO_3^+, $SO^+/H_2SO_4^+$, SO_2^+/SO_3^+, SO_2^+/HSO_3^+, and $SO_2^+/H_2SO_4^+$ ratios to explore possible HMS contributions to the organic aerosol in question (Ge et al., 2012), where higher ratios indicate higher amounts of HMS in the ambient aerosol. Of these ratios, $SO^+/H_2SO_4^+$ and $SO_2^+/H_2SO_4^+$ fluctuate most dramatically over time (and between fog and non-fog periods; Fig. S5). $SO_2^+/H_2SO_4^+$ is used herein (Fig. 5). Both the organic mass and $SO_2^+/H_2SO_4^+$ ratio increased after the 7/18 fog episode even though the latter did not to a significant extent. This $SO_2^+/H_2SO_4^+$ increase may arise from a decrease in inorganic SO_4^{2-} (as indicated by the decrease in the mass of total SO_4^{2-}) and/or real increase in the HMS contribution, but may also be changed within error. Nonetheless, the change in this ratio suggests that the aqueous-phase SOA contributions increased in importance relative to inorganic SO_4^{2-} during this episode. $SO_2^+/H_2SO_4^+$ did not increase along with organic mass on 7/2, but NO_3^- did. This concurrent increase in organics and NO_3^- may indicate the formation of organonitrates, which can contribute to the SOA mass increases in atmospheric droplets.

Table 2
Positive Matrix Factorization (PMF) analysis of organics before and after fog event. PMF-OA was separated by 3-factors, which was HOA, LO-OOA, and MO-OOA.

Date (2014)	PMF-OA[a]		HOA[b]		LO-OOA[b]		MO-OOA[b]	
	Before	After	Before	After	Before	After	Before	After
June 30th	1.62	1.67	0.04	0.10	0.40	0.52	0.56	0.39
July 1st	0.86	0.57	0.11	0.16	0.17	0.16	0.72	0.68
July 2nd	1.96	3.02	0.08	0.07	0.29	0.48	0.63	0.46
July 18th	0.17	0.27	0.39	0.42	0.35	0.58	0.27	0.00
July 20th	0.55	0.23	0.55	0.89	0.06	0.00	0.38	0.11

[a] Absolute concentration, μg m^{-3}.
[b] Fraction of PMF-OA.

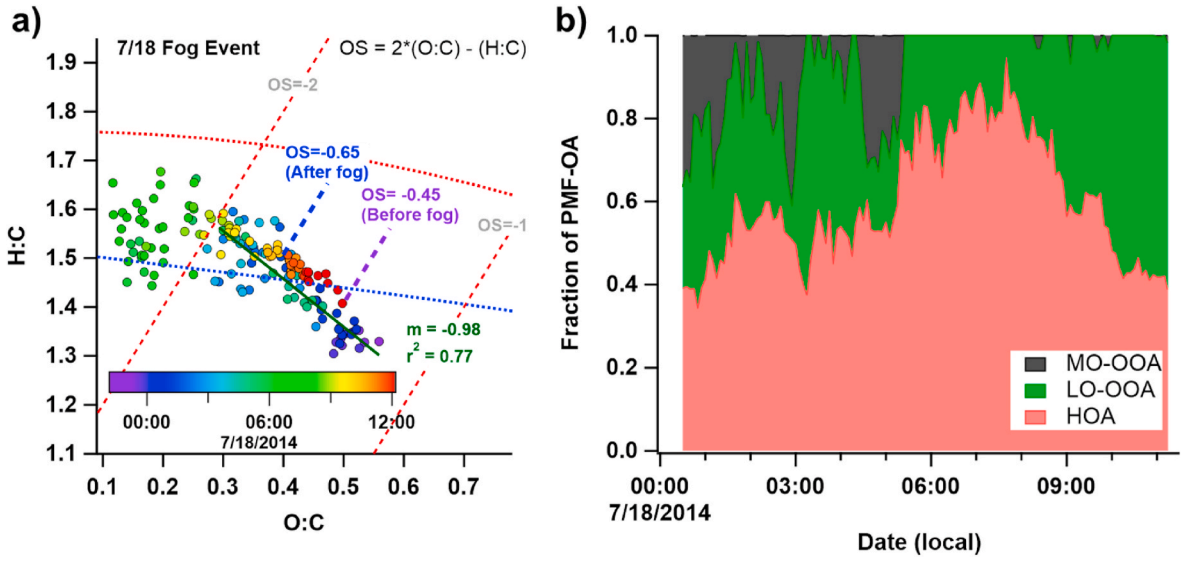

Fig. 7. a) van Krevelen diagram showing changes in organic oxidation and b) fraction of PMF-OA about 3-factors during the 7/18 fog event. The dark green line shows a linear regression through the data points within the fog event in Fig. 7a). (For interpretation of the references to colour in this figure legend, the reader is referred to the Web version of this article.)

3.5. Changes in aerosol oxidation state after fog events

As shown in Fig. 6, the aerosol carbon oxidation state was lower after the fog event than before the fog onset for all fog episodes. In addition, we separated OA into 3-factors as HOA, LO-OOA, and MO-OOA (Figs. S2 and S3). The HOA is similar to Primary OA (POA), LO-OOA and MO-OOA correspond to SOA (Zhang et al., 2011). The MO-OOA decreased after fog in all fog episodes, but relatively fresh LO-OOA and HOA increased (Table 2). The HOA increased in all cases except 7/2, and LO-OOA increased in 6/30, 7/2, and 7/18 cases. The carbon oxidation state of after fog event in 7/20 case was the lowest of five episodes (Fig. 6). In addition, the highest HOA and lowest SOA (LO-OOA + MO-OOA) ratios were observed after fog compared to other cases. This phenomenon suggests that the processing of SOA precursors forms less-oxidized SOA and/or causes the fragmentation and loss of oxidized functional groups, which can occur during aqueous photooxidation (Schurman et al., 2018). Such changes in oxidation are often enabled by the uptake of high-order unsaturated VOCs such as light aromatics (e.g., toluene and benzene) and biogenic VOCs (e.g., isoprene), which are subsequently oxidized via aqueous reactions (McNeill, 2015). The resulting semi-volatile SOA can then be released into the particle phase via droplet evaporation (Ervens et al., 2011). In addition, OA increases its hygroscopicity as it is oxidized (Massoli et al., 2010). Massoli et al. (2010) reported that the LV-OOA had higher hygroscopicity than the semi-volatility OOA (SV-OOA) in laboratory SOA experiments. Xu et al. (2017) reported the water-solubility of various OA factors calculated by the PMF. The HOA had the lowest water-solubility, followed by the LO-OOA and the MO-OOA, where oxidation proceeds (Xu et al., 2017). The increase in hygroscopicity of OA creates conditions for increased absorption and growth in fog droplets during fog events (Ming and Russell, 2004). The OA absorbed in fog droplets can be easier to scavenge by wet deposition in the atmosphere, which may increase the proportion of relatively fresh OA by scavenged OA.

During the 7/18 event, which featured the most notable change in carbon oxidation state and overall decreases in all particle components, the organic content developed lower O:C and higher H:C over the course of the fog episode indicating a decrease in oxidation (Fig. 7a). This oxidation process clearly falls along a slope of −1 (see linear regression for the fog period in dark green), which is indicative of carboxylic acid or hydroxycarbonyl loss (when moving "up" the line toward higher H:C and lower O:C; Heald et al., 2010). In addition, during fog events, H:C and the fraction of HOA was increased and then decreased, while O:C and the fraction of SOA decreased and only O:C and LO-OOA increased (Fig. 7). This behavior is consistent with particles produced from drying aerosolized cloud water during laboratory photooxidation (Schurman et al., 2018). Interestingly, although not as relevant to the discussion of fog aerosol processing herein, the particles follow approximately the same slope toward higher O:C and lower H:C after the fog event as they are re-oxidized in the atmosphere, which is likely by adding carboxylic acid or hydroxycarbonyl groups (Fig. 7b).

3.6. Changes in aerosol physical properties during fog

The particle size distribution and size-resolved chemical compositions before (02:30–03:00 h) and after (08:00–08:30 h) the 6/30 fog event were compared (Fig. 8 and Fig. S6). Unfortunately, the analysis

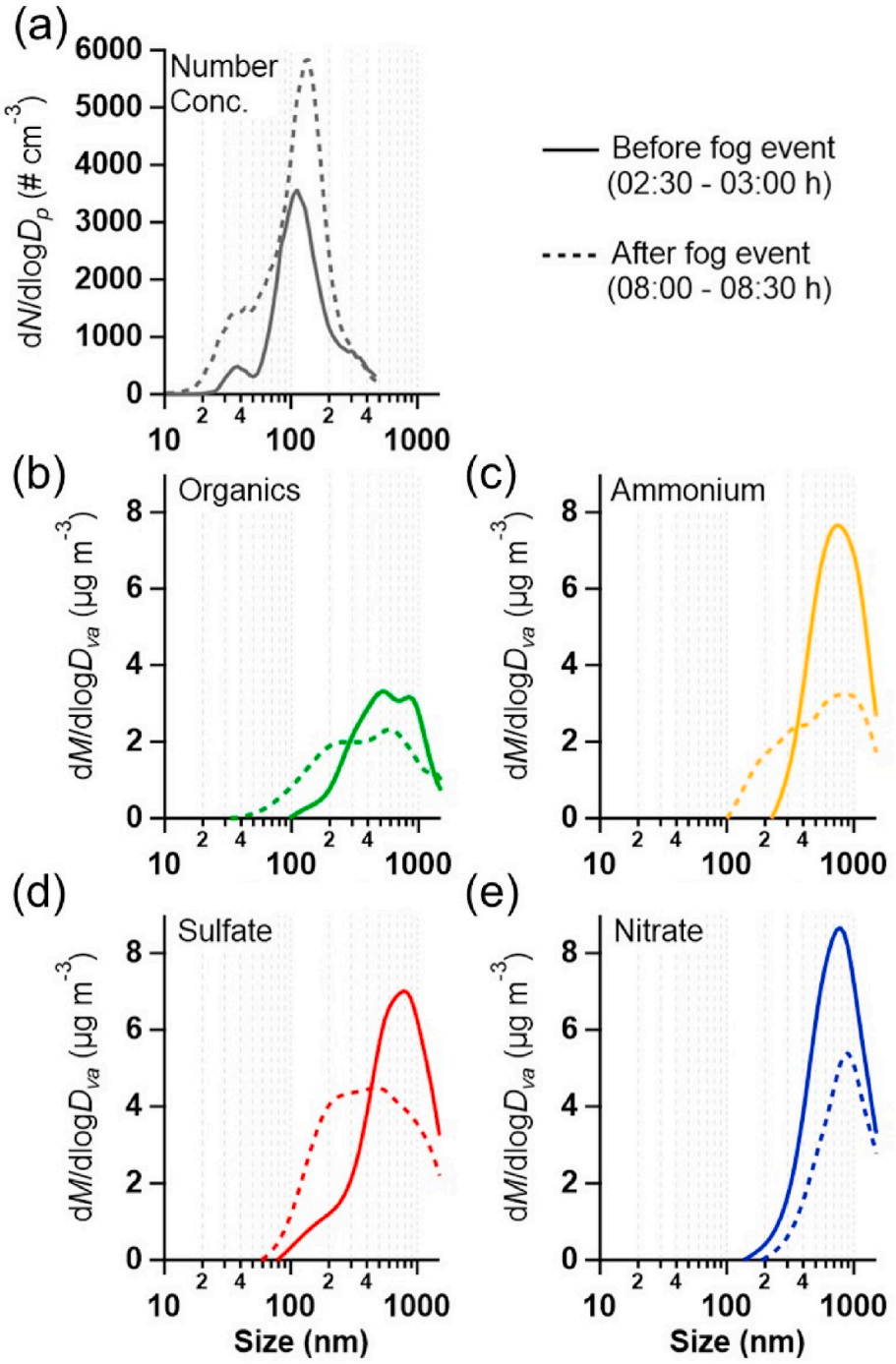

Fig. 8. Particle size distributions (a) and size-resolved chemical compositions (b, c, d, and e) before and after the fog event on 6/30. (a) Size range was 10.4–469.8 nm as measured by SMPS. (b, c, d, and e) Size range was 40–1000 nm as measured by HR-ToF-AMS.

range of the SMPS was 10.4–469.8 nm, which could not be precisely compared with that of the HR-ToF-AMS, but it was used for understanding the particle distribution below 500 nm (Fig. 8a). The mode diameter before the fog event was 111.4 nm (3566 particles cm^{-3}), and the mode diameter increased to 138.2 nm (5831 particles cm^{-3}) after the fog event. The increase in the number of particles was observed to be below the 300 nm size. The all size-resolved chemical composition of NR-PM_1 were decreased within the 300–1000 nm (Fig. 8b–e) particle range, probably because of wet deposition. The concentrations of Org, SO_4^{2-}, and NH_4^+ were increased below 300 nm. The concentration of NO_3^- did not increase below 300 nm after the fog event. During the fog event, gaseous compounds (e.g., VOCs, H_2SO_4, and NH_3) react to the condensation mode particles (Ge et al., 2012), and secondary aerosol, such as $(NH_4)_2SO_4$ and NH_4HSO_4, is formed by aqueous phase reactions in the fog droplet. This supports the increase in Org, NO_3^-, SO_4^{2-}, and number concentrations below 300 nm (Fig. 8). In addition, the correlation between SO_4^{2-} and NH_4^+ after the fog event was observed to be 0.82 (correlation coefficient), while the correlation between NO_3^- and NH_4^+ was 0.2, suggesting internal mixing of SO_4^{2-} and NH_4^+ in the particle.

4. Conclusions

The aerosol physical and chemical measurements were conducted at

the Baengnyeong Island Intensive Air Quality Monitoring Station, South Korea during June–July 2014. The chemical composition and physical properties of aerosol particles were characterized before, during (interstitial), and after fog events using a high-resolution time of flight aerosol mass spectrometer (HR-ToF-AMS) and scanning mobility particle sizer (SMPS). Five fog episodes on 6/30, 7/1, 7/2, 7/18, and 7/20 were analyzed.

Total NR-PM_1 averaged 4.86 ± 4.36 μg m^{-3} during fog episodes (representing the unscavenged interstitial aerosol) and 6.30 ± 4.26 μg m^{-3} during non-fog periods, decreasing by an average of 22.8% with the onset of a fog event. The organic aerosol scavenging efficiency was 7–34%, with lower η associated with lower organic oxidation (and thus, hygroscopicity), while that for ammonia measured 16–68%, for SO_4^{2-} from −1 (indicating a slight increase in mass) to 35%, and that for NO_3^- 17–86%. This enhanced NO_3^- scavenging phenomenon is consistent with previous studies and the relatively high hygroscopicity of NO_3^-. For both Org and NO_3^-, the variation in scavenging may also be size dependent as has been found previously. The particles were smaller (mode = 346 nm) on 7/18, when the NO_3^- η values were smaller, and larger (593 nm) during the higher NO_3^- η event on 7/1.

Changes in component mass were also explored before and after fog events. While three episodes featured overall decreases in component mass after the conclusion of the fog event, two episodes feature overall increases in mass, most notably in organics, despite the initial scavenging. Potential evidence was seen for aqSOA formation, including possible HMS and organonitrate formation. HMS formation would likely be greater in higher pH fogs than in these episodes.

The aerosol carbon oxidation state was lower after all fog episodes suggesting the processing of SOA precursors to form less-oxidized SOA, potential loss by fog deposition of scavenged highly oxidized organics, and/or fragmentation and loss of oxidized functional groups, which can occur during aqueous photooxidation. During the 7/18 event, which featured the most notable change in carbon oxidation state and particle component decreases, the organic content developed lower O:C and higher H:C over the course of the fog episode indicating a decrease in oxidation. This process clearly progresses "up" a slope of −1 in the van Krevelen diagram, indicative of carboxylic acid or hydroxycarbonyl loss, which is consistent with particles produced from drying aerosolized cloud water during laboratory photooxidation.

Study shortcomings include difficulty in differentiating changes in particle chemistry due to fog interactions from those due to air mass transport. Therefore, future studies might constrain this by monitoring particle composition just upwind of the fog area and comparing variations therein to changes in the interstitial particles and particles released by evaporating fog droplets (e.g., as might be studied in an orographic cloud). The collection of parallel gas-phase precursor data would enable a comparison between formed (or lost) OA and consumed (or released) gaseous species, thereby, enabling a much more complete picture of fog scavenging in all possible phases.

CRediT authorship contribution statement

Taehyun Park: Writing – original draft, Formal analysis, Investigation. **Dong Hee Jung:** Writing – review & editing, Formal analysis. **Yongjae Lim:** Writing – review & editing, Methodology. **Jihee Ban:** Writing – review & editing, Investigation, Visualization. **Kyunghoon Kim:** Visualization, Validation. **Seokwon Kang:** Visualization, Validation. **Gyutae Park:** Writing – review & editing, Software. **Siyoung Choi:** Visualization. **Hyunjae Kim:** Resources. **Minyoung Sung:** Resources. **Yongjoo Choi:** Writing – review & editing. **Alexandra J. Boris:** Writing – review & editing. **Jeffrey L. Collett:** Jr, Writing – review & editing. **Taehyoung Lee:** Conceptualization, Supervision, Project administration, Writing – original draft.

Declaration of competing interest

The authors declare that they have no known competing financial interests or personal relationships that could have appeared to influence the work reported in this paper.

Acknowledgements

This work was supported by grants from the National Research Foundation of Korea (Grant No. NRF-2014R1A1A1007947). The additional data analysis was supported by the National Institute of Environmental Research (NIER-2020-04-02-006) and the extended experiment was conducted by Korea Basic Science Institute (National research Facilities and Equipment Center) grant funded by the Ministry of Education (2019R1A6C1020041).

Appendix A. Supplementary data

Supplementary data to this article can be found online at https://doi.org/10.1016/j.atmosenv.2022.119091.

References

Aiken, A.C., Decarlo, P.F., Kroll, J.H., Worsnop, D.R., Huffman, J.A., Docherty, K.S., Ulbrich, I.M., Mohr, C., Kimmel, J.R., Sueper, D., Sun, Y., Zhang, Q., Trimborn, A., Northway, M., Ziemann, P.J., Canagaratna, M.R., Onasch, T.B., Alfarra, M.R., Prevot, A.S.H., Dommen, J., Duplissy, J., Metzger, A., Baltensperger, U., Jimenez, J. L., 2008. O/C and OM/OC ratios of primary, secondary, and ambient organic aerosols with high-resolution time-of-flight aerosol mass spectrometry. Environ. Sci. Technol. 42, 4478–4485. https://doi.org/10.1021/es703009q.

Allan, J.D., Delia, A.E., Coe, H., Bower, K.N., Alfarra, M.R., Jimenez, J.L., Middlebrook, A.M., Drewnick, F., Onasch, T.B., Canagaratna, M.R., Jayne, J.T., Worsnop, D.R., 2004. A generalised method for the extraction of chemically resolved mass spectra from Aerodyne aerosol mass spectrometer data. J. Aerosol Sci. 35, 909–922. https://doi.org/10.1016/j.jaerosci.2004.02.007.

Benedict, K.B., Kreidenweis, S.M., Schichtel, B., Malm, W.C., Carrico, C., Collett Jr., J.L., 2013. A seasonal nitrogen deposition budget for Rocky Mountain National Park. Ecol. Appl. 23, 1156–1169. https://doi.org/10.1890/12-1624.1.

Boris, A.J., Lee, T., Park, T., Choi, J., Seo, S.J., Collett Jr., J.L., 2016. Fog composition at Baengnyeong Island in the eastern Yellow Sea: detecting markers of aqueous atmospheric oxidations. Atmos. Chem. Phys. 16, 437–453. https://doi.org/10.5194/acp-16-437-2016.

Canagaratna, M.R., Jimenez, J.L., Kroll, J.H., Chen, Q., Kessler, S.H., Massoli, P., Hildebrandt Ruiz, L., Fortner, E., Williams, L.R., Wilson, K.R., Surratt, J.D., Donahue, N.M., Jayne, J.T., Worsnop, D.R., 2015. Elemental ratio measurements of organic compounds using aerosol mass spectrometry: characterization, improved calibration, and implications. Atmos. Chem. Phys. 15, 253–272. https://doi.org/10.5194/acp-15-253-2015.

Carlton, A.G., Turpin, B.J., Altieri, K.E., Seitzinger, S., Reff, A., Lim, H.-J., Ervens, B., 2007. Atmospheric oxalic acid and soa production from glyoxal: results of aqueous photooxidation experiments. Atmos. Environ. 41, 7588–7602. https://doi.org/10.1016/j.atmosenv.2007.05.035.

Choi, J.-S., Kim, J.-H., Lee, T.-H., Choi, Y.-J., Park, T.-H., Oh, J., Park, in-S., Ahn, J.-Y., Jeon, H.-E., Koo, Y.-S., Kim, S.-D., Hong, Y.-D., Hong, J.-H., 2016. A study on chemical characteristics of aerosol composition at west inflow regions in the Korean Peninsula I. Characteristics of PM concentration and chemical components. J. Korean Soc. Atmos. Environ. 32, 469–484. https://doi.org/10.5572/KOSAE.2016.32.5.469.

Choi, Y., Rhee, T.S., Collett, J.L., Park, T., Park, S.-M., Seo, B.-K., Park, G., Park, K., Lee, T., 2017. Aerosol concentrations and composition in the North Pacific marine boundary layer. Atmos. Environ. 171, 165–172. https://doi.org/10.1016/J.ATMOSENV.2017.09.047.

Collett, J.L., Herckes, P., Youngster, S., Lee, T., 2008. Processing of atmospheric organic matter by California radiation fogs. Atmos. Res. 87, 232–241. https://doi.org/10.1016/j.atmosres.2007.11.005.

Collett, J.L.J., Sherman, D.E., Moore, K.F., Hannigan, M.P., Lee, T., 2001. Aerosol particle processing and removal by fogs: observations in chemically heterogeneous central California radiation fogs. Water, air soil pollut. Focus 1, 303–312. https://doi.org/10.1023/A:1013175709931.

Crahan, K.K., Hegg, D., Covert, D.S., Jonsson, H., 2004. An exploration of aqueous oxalic acid production in the coastal marine atmosphere. Atmos. Environ. 38, 3757–3764. https://doi.org/10.1016/j.atmosenv.2004.04.009.

Croft, P.J., Ward, B., 2015. Clouds and fog | fog. In: North, G.R., Pyle, J., Zhang, F. (Eds.), Encyclopedia of Atmospheric Sciences, second ed. Academic Press, Oxford, pp. 180–188. https://doi.org/10.1016/B978-0-12-382225-3.00152-3.

DeCarlo, P., Kimmel, J.R., Trimborn, A.M., Northway, M.J., Jayne, J.T., Aiken, A.C., Gonin, M., Fuhrer, K., Horvath, T., Docherty, K.S., Worsnop, D.R., Jimenez, J.L., 2006. Field-Deployable, High-Resolution, Time-Of-Flight Aerosol Mass Spectrometer. https://doi.org/10.1021/AC061249N.

Decesari, S., Facchini, M.C., Fuzzi, S., McFiggans, G.B., Coe, H., Bower, K.N., 2005. The water-soluble organic component of size-segregated aerosol, cloud water and wet depositions from Jeju Island during ACE-Asia. Atmos. Environ. 39, 211–222. https://doi.org/10.1016/j.atmosenv.2004.09.049.

Elias, T., Dupont, J.C., Hammer, E., Hoyle, C.R., Haeffelin, M., Burnet, F., Jolivet, D., 2015. Enhanced extinction of visible radiation due to hydrated aerosols in mist and fog. Atmos. Chem. Phys. 15, 6605–6623. https://doi.org/10.5194/acp-15-6605-2015.

Ervens, B., 2015. Modeling the processing of aerosol and trace gases in clouds and fogs. Chem. Rev. 115, 4157–4198. https://doi.org/10.1021/cr5005887.

Ervens, B., Turpin, B.J., Weber, R.J., 2011. Secondary organic aerosol formation in cloud droplets and aqueous particles (aqSOA): a review of laboratory, field and model studies. Atmos. Chem. Phys. 11, 11069–11102. https://doi.org/10.5194/acp-11-11069-2011.

Farmer, D.K., Matsunaga, A., Docherty, K.S., Surratt, J.D., Seinfeld, J.H., Ziemann, P.J., Jimenez, J.L., 2010. Response of an aerosol mass spectrometer to organonitrates and organosulfates and implications for atmospheric chemistry. Proc. Natl. Acad. Sci. Unit. States Am. 107, 6670–6675. https://doi.org/10.1073/pnas.0912340107.

Ge, X., Zhang, Q., Sun, Y., Ruehl, C.R., Setyan, A., 2012. Effect of aqueous-phase processing on aerosol chemistry and size distributions in Fresno, California, during wintertime. Environ. Chem. 9, 221. https://doi.org/10.1071/EN11168.

Gerber, H., 1991. Direct measurement of suspended particulate volume concentration and far-infrared extinction coefficient with a laser-diffraction instrument. Appl. Opt. 30, 4824–4831. https://doi.org/10.1364/AO.30.004824.

Ghan, S.J., Schwartz, S.E., Ghan, S.J., Schwartz, S.E., 2007. Aerosol properties and processes: a path from field and laboratory measurements to global climate models. Bull. Am. Meteorol. Soc. 88, 1059–1084. https://doi.org/10.1175/BAMS-88-7-1059.

Gilardoni, S., Massoli, P., Giulianelli, L., Rinaldi, M., Paglione, M., Pollini, F., Lanconelli, C., Poluzzi, V., Carbone, S., Hillamo, R., Russell, L.M., Facchini, M.C., Fuzzi, S., 2014. Fog scavenging of organic and inorganic aerosol in the Po Valley. Atmos. Chem. Phys. 14, 6967–6981. https://doi.org/10.5194/acp-14-6967-2014.

Harris, E., Sinha, B., Van Pinxteren, D., Schneider, J., Poulain, L., Collett, J., D'Anna, B., Fahlbusch, B., Foley, S., Fomba, K., 2014. In-cloud sulfate addition to single particles resolved with sulfur isotope analysis during HCCT-2010. Chem. Phys. 14, 4219–4235. https://doi.org/10.5194/acp-14-4219-2014.

Heald, C.L., Kroll, J.H., Jimenez, J.L., Docherty, K.S., DeCarlo, P.F., Aiken, A.C., Chen, Q., Martin, S.T., Farmer, D.K., Artaxo, P., 2010. A simplified description of the evolution of organic aerosol composition in the atmosphere. Geophys. Res. Lett. 37 https://doi.org/10.1029/2010GL042737.

Herckes, P., Valsaraj, K.T., Collett, J.L., 2013. A review of observations of organic matter in fogs and clouds: origin, processing and fate. Atmos. Res. https://doi.org/10.1016/j.atmosres.2013.06.005.

Hering, S.V., Friedlander, S.K., 1982. Origins of aerosol sulfur size distributions in the Los Angeles basin. Atmos. Environ. 16, 2647–2656. https://doi.org/10.1016/0004-6981(82)90346-8.

Hogrefe, O., Lala, G.G., Frank, B.P., Schwab, J.J., Demerjian, K.L., 2006. Field evaluation of a TSI model 3034 scanning mobility particle sizer in New York city: winter 2004 intensive campaign. Aerosol Sci. Technol. 40, 753–762. https://doi.org/10.1080/02786820600721846.

Jimenez, J., Canagaratna, M., Donahue, N., Prevot, A., Zhang, Q., Kroll, J., DeCarlo, P., Allan, J., Coe, H., Ng, N., 2009. Evolution of organic aerosols in the atmosphere. Science 326, 1525–1529. https://doi.org/10.1126/science.1180353.

John, W., Wall, S.M., Ondo, J.L., Winklmayr, W., 1990. Modes in the size distributions of atmospheric inorganic aerosol. Atmos. Environ. Part A. Gen. Top. 24, 2349–2359. https://doi.org/10.1016/0960-1686(90)90327-J.

Kang, E., Lee, M., Brune, W.H., Lee, T., Park, T., Ahn, J., Shang, X., 2018. Photochemical aging of aerosol particles in different air masses arriving at Baengnyeong Island, Korea. Atmos. Chem. Phys. 18, 6661–6677. https://doi.org/10.5194/acp-18-6661-2018.

Kang, S., Park, G., Park, T., Ban, J., Kim, K., Seo, Y., Choi, J., Seo, S., Choi, J., Bae, M., Lee, T., 2020. Semi-continuous measurements of water-soluble organic carbon and ionic composition of PM2.5 in Baengnyeong Island during the 2016 KORUS-AQ. Asian. J. Atmos. Environ. 14, 307–318. https://doi.org/10.5572/ajae.2020.14.3.307.

Kaul, D.S., Gupta, T., Tripathi, S.N., Tare, V., Collett, J.L., 2011. Secondary organic aerosol: a comparison between foggy and nonfoggy days. Environ. Sci. Technol. 45, 7307–7313. https://doi.org/10.1021/es201081d.

Korea Meteorological Administration, 2022. Automated Synoptic Observing System (ASOS) Data. URL. https://data.kma.go.kr/data/grnd/selectAsosRltmList.do?pgmNo=36.

Kroll, J.H., Smith, J.D., Che, D.L., Kessler, S.H., Worsnop, D.R., Wilson, K.R., 2009. Measurement of fragmentation and functionalization pathways in the heterogeneous oxidation of oxidized organic aerosol. Phys. Chem. Chem. Phys. 11, 8005–8014. https://doi.org/10.1039/b905289e.

Lambe, A.T., Ahern, A.T., Williams, L.R., Slowik, J.G., Wong, J.P.S., Abbatt, J.P.D., Brune, W.H., Ng, N.L., Wright, J.P., Croasdale, D.R., Worsnop, D.R., Davidovits, P., Onasch, T.B., 2011. Characterization of aerosol photooxidation flow reactors: heterogeneous oxidation, secondary organic aerosol formation and cloud condensation nuclei activity measurements. Atmos. Meas. Tech. 4, 445–461. https://doi.org/10.5194/amt-4-445-2011.

Lee, T., Choi, J., Lee, G., Ahn, J., Park, J.S., Atwood, S.A., Schurman, M., Choi, Y., Chung, Y., Collett, J.L., 2015. Characterization of aerosol composition, concentrations, and sources at Baengnyeong Island, Korea using an aerosol mass spectrometer. Atmos. Environ. 120, 297–306. https://doi.org/10.1016/J.ATMOSENV.2015.08.038.

Liu, P.S.K., Deng, R., Smith, K.A., Williams, L.R., Jayne, J.T., Canagaratna, M.R., Moore, K., Onasch, T.B., Worsnop, D.R., Deshler, T., 2007. Transmission efficiency of an aerodynamic focusing lens system: comparison of model calculations and laboratory measurements for the aerodyne aerosol mass spectrometer. Aerosol Sci. Technol. 41, 721–733. https://doi.org/10.1080/02786820701422278.

Massoli, P., Lambe, A.T., Ahern, A.T., Williams, L.R., Ehn, M., Mikkilä, J., Canagaratna, M.R., Brune, W.H., Onasch, T.B., Jayne, J.T., Petäjä, T., Kulmala, M., Laaksonen, A., Kolb, C.E., Davidovits, P., Worsnop, D.R., 2010. Relationship between aerosol oxidation level and hygroscopic properties of laboratory generated secondary organic aerosol (SOA) particles. Geophys. Res. Lett. 37, L24801. https://doi.org/10.1029/2010GL045258.

McNeill, V.F., 2015. Aqueous organic chemistry in the atmosphere: sources and chemical processing of organic aerosols. Environ. Sci. Technol. 49, 1237–1244. https://doi.org/10.1021/es5043707.

Middlebrook, A.M., Bahreini, R., Jimenez, J.L., Canagaratna, M.R., 2012. Evaluation of composition-dependent collection efficiencies for the aerodyne aerosol mass spectrometer using field data. Aerosol Sci. Technol. 46, 258–271. https://doi.org/10.1080/02786826.2011.620041.

Ming, Y., Russell, L.M., 2004. Organic aerosol effects on fog droplet spectra. J. Geophys. Res. Atmos. 109, D10206. https://doi.org/10.1029/2003JD004427.

Munger, J.W., Tiller, C., Hoffmann, M., 1986. Identification of hydroxymethanesulfonate in fog water. Science 231 (4735), 247–249. https://doi.org/10.1126/science.231.4735.247.

Ng, N.L., Canagaratna, M.R., Zhang, Q., Jimenez, J.L., Tian, J., Ulbrich, I.M., Kroll, J.H., Docherty, K.S., Chhabra, P.S., Bahreini, R., Murphy, S.M., Seinfeld, J.H., Hildebrandt, L., Donahue, N.M., DeCarlo, P.F., Lanz, V.A., Prévôt, A.S.H., Dinar, E., Rudich, Y., Worsnop, D.R., 2010. Organic aerosol components observed in northern hemispheric datasets from aerosol mass spectrometry. Atmos. Chem. Phys. 10, 4625–4641. https://doi.org/10.5194/acp-10-4625-2010.

Noone, K.J., Ogren, J.A., Hallberg, A., Heintzenberg, J., StrÖm, J., Hansson, H.-C., Svenningsson, B., Wiedensohler, A., Fuzzi, S., Facchini, M.C., Arends, B.G., Berner, A., 1992. Changes in aerosol size- and phase distributions due to physical and chemical processes in fog. Tellus B 44, 489–504. https://doi.org/10.3402/tellusb.v44i5.15563.

Phinney, L., Richard Leaitch, W., Lohmann, U., Boudries, H., Worsnop, D.R., Jayne, J.T., Toom-Sauntry, D., Wadleigh, M., Sharma, S., Shantz, N., 2006. Characterization of the aerosol over the sub-arctic north east Pacific Ocean. Deep Sea Res. Part II Top. Stud. Oceanogr. 53, 2410–2433. https://doi.org/10.1016/J.DSR2.2006.05.044.

Paatero, P., 1997. Least squares formulation of robust non-negative factor Analysis. Chemometr. Intell. Lab. Syst. 37, 23–35. https://doi.org/10.1016/S0169-7439(96)00044-5.

Paatero, P., Tapper, U., 1994. Positive matrix factorization: a non-negative factor model with optimal utilization of error estimates of data values. Environmetrics 5, 111–126. https://doi.org/10.1002/env.3170050203.

Pope III, C.A., Burnett, R.T., Thun, M.J., Calle, E.E., Krewski, D., Ito, K., Thurston, G.D., 2002. Lung cancer, cardiopulmonary mortality, and long-term exposure to fine particulate air pollution. JAMA 287, 1132. https://doi.org/10.1001/jama.287.9.1132.

Pruppacher, H.R., Klett, J.D., 2010. Microstructure of atmospheric clouds and precipitation. In: Microphysics of Clouds and Precipitation. Springer, Dordrecht.

Rivellini, L.-H., Chiapello, I., Tison, E., Fourmentin, M., Féron, A., Diallo, A., N& apos, Diaye, T., Goloub, P., Canonaco, F., Prévôt, A.S.H., Riffault, V., 2017. Chemical characterization and source apportionment of submicron aerosols measured in Senegal during the 2015 SHADOW campaign. Atmos. Chem. Phys. 17, 10291–10314. https://doi.org/10.5194/acp-17-10291-2017.

Saarikoski, S., Carbone, S., Decesari, S., Giulianelli, L., Angelini, F., Canagaratna, M., Ng, N.L., Trimborn, A., Facchini, M.C., Fuzzi, S., Hillamo, R., Worsnop, D., 2012. Chemical characterization of springtime submicrometer aerosol in Po valley, Italy. Atmos. Chem. Phys. 12, 8401–8421. https://doi.org/10.5194/acp-12-8401-2012.

Schulze, B.C., Wallace, H.W., Bui, A.T., Flynn, J.H., Erickson, M.H., Alvarez, S., Dai, Q., Usenko, S., Sheesley, R.J., Griffin, R.J., 2018. The impacts of regional shipping emissions on the chemical characteristics of coastal submicron aerosols near Houston, TX. Atmos. Chem. Phys. Discuss. 1–63. https://doi.org/10.5194/acp-2018-509.

Schurman, M.I., Boris, A., Desyaterik, Y., Collett, J.L., 2018. Aqueous secondary organic aerosol formation in ambient cloud water photo-oxidations. Aerosol Air Qual. Res. 18, 15–25. https://doi.org/10.4209/aaqr.2017.01.0029.

Sellegri, K., Laj, P., Dupuy, R., Legrand, M., Preunkert, S., Putaud, J.-P., 2003. Size-dependent scavenging efficiencies of multicomponent atmospheric aerosols in clouds. J. Geophys. Res. 108, 4334. https://doi.org/10.1029/2002JD002749.

Shen, X., Lee, T., Guo, J., Wang, X., Li, P., Xu, P., Wang, Y., Ren, Y., Wang, W., Wang, T., 2012. Aqueous phase sulfate production in clouds in eastern China. Atmos. Environ. 62, 502–511. https://doi.org/10.1016/j.atmosenv.2012.07.079.

Sueper, D., 2009. ToF-AMS High Resolution Analysis Software [WWW Document]. URL. http://cires.colorado.edu/jimenez-group/ToFAMSResources/ToFSoftware/index.%0Dhtml.

Sun, Y.L., Zhang, Q., Schwab, J.J., Demerjian, K.L., Chen, W.N., Bae, M.S., Hung, H.M., Hogrefe, O., Frank, B., Rattigan, O.V., Lin, Y.C., 2011. Characterization of the sources and processes of organic and inorganic aerosols in New York city with a high-resolution time-of-flight aerosol mass apectrometer. Atmos. Chem. Phys. 11, 1581–1602. https://doi.org/10.5194/acp-11-1581-2011.

Tang, I.N., Munkelwitz, H.R., 1993. Composition and temperature dependence of the deliquescence properties of hygroscopic aerosols. Atmos. Environ. Part A. Gen. Top. 27, 467–473. https://doi.org/10.1016/0960-1686(93)90204-C.

Ulbrich, I.M., Canagaratna, M.R., Zhang, Q., Worsnop, D.R., Jimenez, J.L., 2009. Interpretation of organic components from positive matrix factorization of aerosol

mass spectrometric data. Atmos. Chem. Phys. 9, 2891–2918. https://doi.org/10.5194/acp-9-2891-2009.

van Pinxteren, D., Fomba, K.W., Mertes, S., Müller, K., Spindler, G., Schneider, J., Lee, T., Collett, J., Herrmann, H., 2016. Cloud water composition during HCCT-2010: scavenging efficiencies, solute concentrations, and droplet size dependence of inorganic ions and dissolved organic carbon. Atmos. Chem. Phys. 16, 3185–3205. https://doi.org/10.5194/acp-16-3185-2016.

Varutbangkul, V., Brechtel, F.J., Bahreini, R., Ng, N.L., Keywood, M.D., Kroll, J.H., Flagan, R.C., Seinfeld, J.H., Lee, A., Goldstein, A.H., 2006. Hygroscopicity of secondary organic aerosols formed by oxidation of cycloalkenes, monoterpenes, sesquiterpenes, and related compounds. Atmos. Chem. Phys. 6, 2367–2388. https://doi.org/10.5194/acp-6-2367-2006.

von Glasow, R., Crutzen, P.J., 2004. Model study of multiphase DMS oxidation with a focus on halogens. Atmos. Chem. Phys. 4, 589–608. https://doi.org/10.5194/acp-4-589-2004.

Weber, R.J., Sullivan, A.P., Peltier, R.E., Russell, A., Yan, B., Zheng, M., de Gouw, J., Warneke, C., Brock, C., Holloway, J.S., Atlas, E.L., Edgerton, E., 2007. A study of secondary organic aerosol formation in the anthropogenic-influenced southeastern United States. J. Geophys. Res. Atmos. 112, D13302. https://doi.org/10.1029/2007JD008408.

Whiteaker, J.R., Prather, K.A., 2003. Hydroxymethanesulfonate as a tracer for fog processing of individual aerosol particles. Atmos. Environ. 37, 1033–1043. https://doi.org/10.1016/S1352-2310(02)01029-4.

Xu, L., Guo, H., Weber, R.J., Ng, N.L., 2017. Chemical characterization of water-soluble organic aerosol in contrasting rural and urban environments in the southeastern United States. Environ. Sci. Technol. 51, 78–88. https://doi.org/10.1021/acs.est.6b05002.

Zhang, Q., Jimenez, J.L., Canagaratna, M.R., Ulbrich, I.M., Ng, N.L., Worsnop, D.R., Sun, Y., 2011. Understanding atmospheric organic aerosols via factor Analysis of aerosol mass spectrometry: a review. Anal. Bioanal. Chem. 401, 3045–3067. https://doi.org/10.1007/s00216-011-5355-y.

Zhao, Y., Hallar, A.G., Mazzoleni, L.R., 2013. Atmospheric organic matter in clouds: exact masses and molecular formula identification using ultrahigh-resolution FT-ICR mass spectrometry. Atmos. Chem. Phys. 13, 12343–12362. https://doi.org/10.5194/acp-13-12343-2013.

Zorn, S.R., Drewnick, F., Schott, M., Hoffmann, T., Borrmann, S., 2008. Characterization of the South Atlantic marine boundary layer aerosol using an aerodyne aerosol mass spectrometer. Atmos. Chem. Phys. 8, 4711–4728. https://doi.org/10.5194/acp-8-4711-2008.